Tapar, O.; Steinbacher, M.; Gibmeier, J.; Schell, N.; Epp, J.:
In situ Investigation during Low Pressure Carburizing by Means of Synchrotron X-ray Diffraction : In-situ-Untersuchung während der Niederdruckaufkohlung mittels Synchrotron-Röntgenbeugung.
In: HTM - Journal of Heat Treatment and Materials. Vol. 76 (2021) 6, 417 - 431.

First published online by Hanser: 31.12.2021

https://dx.doi.org/10.1515/htm-2021-0018

In-situ Investigation during Low Pressure Carburizing by Means of Synchrotron X-ray Diffraction

M. Sc. Ogün Baris Tapar, Leibniz Institute for Materials Engineering, Badgasteiner Str. 3, 28359 Bremen, Germany, tapar@iwt-bremen.de (corresponding author)

Dr.-Ing. Matthias Steinbacher, Leibniz Institute for Materials Engineering, Bremen, Germany
MAPEX Centre for Materials and Processes, Bremen, Germany

Dr.-Ing. Jens Gibmeier, Karlsruhe Institute of Technology, Institute for Applied Materials (IAM), Karlsruhe, Germany

Dr.-Ing. Norbert Schell, Institute of Materials Physics, Helmholtz-Zentrum Hereon, Geesthacht, Germany

Dr.-Ing. Jérémy Epp, Leibniz Institute for Materials Engineering, Bremen, Germany
MAPEX Centre for Materials and Processes, Bremen, Germany

Abstract

In-situ X-ray diffraction investigations during low pressure carburizing (LPC) processes were performed with a specially developed process chamber at the German Electron Synchrotron Facility (DESY) in Hamburg Germany. Carbon saturation in austenite was reached in less than 20 seconds for all processes with different parameters and carbides formed at the surface. Therefore, the direct contribution of carbon donor gas to the carbon profile after 20 seconds was reduced to very low levels. After that point, further supply of carbon donor gas increased the amount of carbides formed at the surface which will contribute to the carbon profile indirectly by dissolution in the following diffusion steps. During quenching, martensite at higher temperatures had a lower c/a ratio than later formed ones. This difference is credited to self-tempering effects and reordering of carbon atoms within the martensite lattice.

Keywords

Low pressure carburizing, synchrotron diffraction, Rietveld refinement, carbon diffusion, carbides

1. Introduction

The combination of a tough core with a high-strength surface layer achieved by carburizing has a positive effect on the wear resistance of technical components [1]. Due to its' high carbon activity which enables large surfaces and also blind holes to be uniformly carburized, low pressure carburizing (LPC), has been gaining importance in industrial manufacturing among standard gas carburizing [2]. Moreover, LPC mostly eliminates oxidation and offers higher quality parts. Additionally, a wide temperature range from 880 °C to 1050 °C shortens

the process time [3], and highly reduced resource consumption, which is primarily due to the very low amount of process gas required [4, 5].

LPC involves creating contact between carbon donor gas and hot metal surface typically in the range of 920-970 °C at low pressure. The typical pressure of the atmosphere in the vacuum-phase is about $5 \cdot 10^{-2}$ mbar and during the process 1-30 mbar. When carbon donor gas is introduced into the furnace under above mentioned conditions, carbon atoms are released, and being absorbed on the steel surface [6]. This step is generally called the boost step and takes place under non-equilibrium conditions since there is a theoretically unlimited carbon supply. Subsequently, the vacuum phase is started by evacuating the remaining gases, in order to let the carbon diffuses towards the core of the steel. Therefore, the carbon content decreases from the surface towards the depth of the sample with solid-state diffusion, which results, in the end, in a characteristic carbon depth profile. This step is generally called the diffusion step. Repetition of boost and diffusion steps can be applied to achieve the desired carbon depth profile. After the desired carbon profile is reached, samples are generally quenched with a high-pressure inert gas such as Helium or Nitrogen or in oil, to get martensitic microstructure. In industry, acetylene (C_2H_2) and propane (C_3H_8) are highly used and the most advantageous gases for LPC [7].

Despite extensive usage of LPC in industry, it still lacks some detailed mechanisms of microstructural evolution and basic understanding. Especially, the mechanism of local carbon enrichment, which leads to successive carbide formation and dissolution during different process steps, is still missing. Therefore, this study aims to give some initial results about the development of a solid solution of carbon, microstructural evolution, carbide formation and carbon diffusion during the LPC process. For this, in-situ synchrotron X-ray diffraction (XRD) experiments in transmission mode were performed during complete LPC including subsequent quenching on Beamline P07-EH3 of the PETRA III Synchrotron at DESY/Hamburg, Germany. Experiments were conducted with different process parameters and the microstructural evolution was evaluated with high spatial and temporal resolution.

2. Material and Experimental Procedure

Standard AISI 5120 (EN 20MnCr5) case hardening steel with 14 mm width, 14 mm height and 5 mm thickness was used as a sample. Annealed state steel rods were used for sample preparation. All samples were cut from same the same direction to minimize the texture effect. The initial microstructure was consisting a homogeneously distributed ferrite-pearlite mixture with an average hardness value of 196 HV. The side surface and bottom surface of the sample were coated with ZrN by using the PVD method in order to suppress the diffusion of carbon from the side surfaces. The effectiveness of the coating was proved by comparing the carbon distribution of carburized coated and uncoated samples [8]. Four SiN heaters, two

on each side of the sample, were used to heat the sample. Beam in/out windows were covered with a 75 µm thick Kapton sheet to allow easy penetration of the X-ray beam [8].

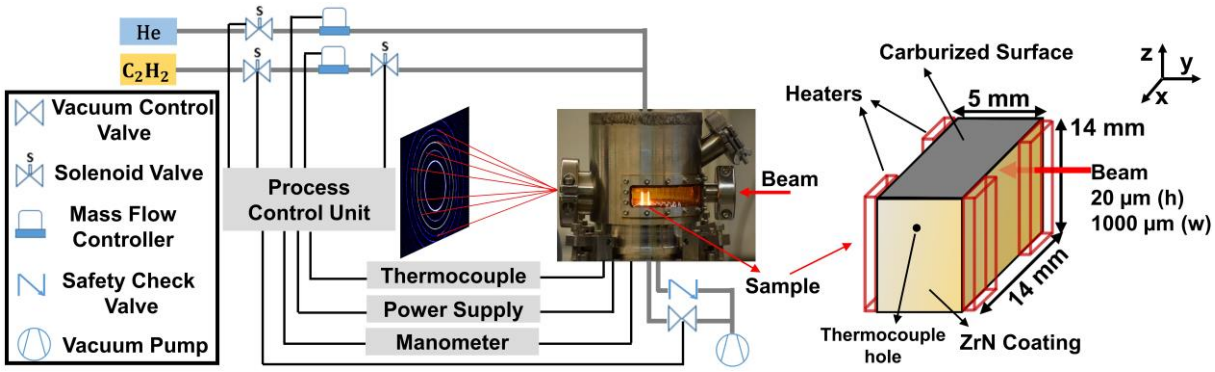

Figure 1: Sketch of the experimental set-up and the sample for in-situ XRD measurement. The beam transmits through a 5 mm depth of the sample heated with 4 heaters and obtained 2D diffraction rings are projected to the 2D Perkin-Elmer detector placed in the beam path.

Figure 1 shows a sketch of the experimental set-up and sample. The diffraction experiments were performed with a high energy monochromatic synchrotron X-ray beam (103.4 keV) for transmission through the whole thickness of the steel sample.

The primary beam height was adjusted to 20 µm to achieve a satisfying spatial resolution in the direction of the carbon gradient. The beam width was chosen as 1000 µm to obtain high signal intensity and good grain statistics. Full diffraction rings were continuously recorded using a 2D detector (Perkin-Elmer XRD 1621 with 2048×2048 px. and a pixel size of 200 µm) placed at 1.32 m behind the sample, while LPC experiments with different process parameters were conducted. The beam was always kept fixed directly at the surface with an acquisition time of 0.2 s/frame during boost and quenching steps. During the diffusion steps, continuous scanning with an acquisition time of 0.5 s/frame over the vertical axis from top to about 500 µm was applied by translating the sample stepwise in vertical z-direction over the fixed beam (see **Figure 1**). Carbon donor gas was acetylene and quench gas was helium for all experiments. All process parameters such as temperature, duration of boost/diffusion steps and flow rate of gases were controlled by a Process Control Unit (PCU).

Recorded 2D patterns were azimuthally integrated for full 360° by using the fast PyFAI software developed at ESRF [9] to obtain conventional 1D diffraction patterns (2θ vs. intensity data). For a detailed analysis of the evolution of lattice parameters and phase fractions, the integrated diffraction patterns were analysed using the convolution-based Rietveld refinement implemented in TOPAS 6.0 Academics [10]. The main focus of the investigation was a change in peak position, since it is the fundamental parameter for the determination of lattice parameters. Thus, local intensity changes e.g. due to the crystallographic texture of the material and the change in peak width were not discussed.

Table 1 shows the process parameters for all samples used in this study. As indicated before, one complete low pressure carburizing process can be separated into 2 main parts as carburizing which covers the boost-diffusion cycle and quenching. For the first part, carburizing, results of 2 consecutive boost-diffusion cycles of four experiments will be given and discussed in the following section (red-edged part of the table). The first one is called as a standard experiment with 940 °C process temperature, 8m^3/m^2h acetylene flow rate and three boost step boost steps (two of them will be given at carburizing part). For the remaining three experiments, process parameters were changed for comparison. For the second part, quenching, the result of standard experiment will be presented and discussed.

Table 1: Process parameters for the experiments

		Boost 1	Diff. 1	Boost 2	Diff. 2	Boost 3	Diff. 3
Standard	**Duration (min)**	1	20	2	20	1	25
	Pressure (mbar)	4	10^{-1}	8	10^{-1}	4	10^{-1}
	Flow rate (m^3/m^2h)	8	0	8	0	8	0
	Temperature (°C)	940	940	940	940	940	940
Experiment 1	**Duration (min)**	1	20	1	20		
	Pressure (mbar)	4	10^{-1}	4	10^{-1}		
	Flow rate (m^3/m^2h)	8	0	8	0		
	Temperature (°C)	920	920	920	920		
Experiment 2	**Duration (min)**	1	20	1	20		
	Pressure (mbar)	4	10^{-1}	4	10^{-1}		
	Flow rate (m^3/m^2h)	8	0	8	0		
	Temperature (°C)	970	970	970	970		
Experiment 3	**Duration (min)**	10	20	10	20		
	Pressure (mbar)	30	10^{-1}	30	10^{-1}		
	Flow rate (m^3/m^2h)	80	0	80	0		
	Temperature (°C)	940	940	940	940		

It can be seen from the table that multiple parameters were varied instead of a single one. One of the reasons for this is that increasing the acetylene amount can be done by either increasing the flow rate and/or duration. Therefore, these two parameters should be considered together. Additionally, the process pressure is linked with boost step duration and cannot be controlled independently. Therefore, only a maximum limit is set as 30 mbar for this parameter with the help of a check valve.

3. Results and Discussion.

3.1. Carburizing

When the sample reached the carburizing temperature of 920 to 970 °C, a successive boost and diffusions cycle was started. **Figure 2** shows the change of main γ {111} austenite peaks positions and change of lattice parameter determined by integration of diffraction pattern during consecutive boost and diffusion steps.

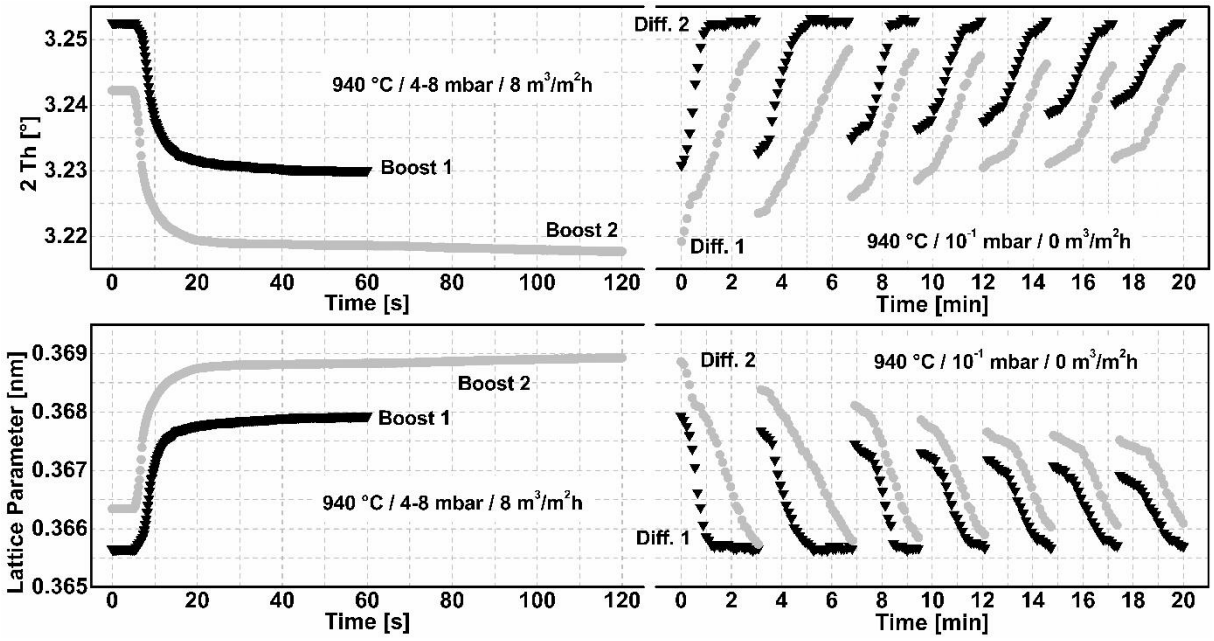

Figure 2: Change of γ {111} austenite peaks position and lattice parameter of austenite vs. time of the γ {111} austenite peak during boost and diffusion steps. Temperature, process pressure and flow rate of acetylene are given on each figure respectively. Error margins are smaller than symbols

According to the figure, when the boost step starts, the austenite peak shift to lower 2θ angles can be clearly observed after about 8 seconds. Peak shifting is very steep in the first couple of seconds and then peak position almost stays constant. In the following diffusion step the during experiment, the sample was scanned from surface to core; therefore, in the figure, a slow shift of the austenite peaks back to higher 2θ angles can be systematically observed both in individual scans and also overall graph. During boost steps, the rapid increase of the lattice parameter is observed at the surface, while during the diffusion step, the lattice parameter at the surface slowly decreases.

There might be chemical, thermal, texture or stress-induced effects as a reason for the observed evolution of the austenite lattice parameters. Without a combination of several measurement methods, it is very difficult to separate these multiple effects precisely. However, samples are in full austenitic range during both boost and diffusion steps with temperatures between 920-970 °C. In that temperature, the effect of stress is expected to be very low; thus, samples can be regarded as stress-free. Additionally, the texture of the material generally affects the intensity of specific peaks due to preferred orientations; however, convolution of the TOPAS covers all peaks which minimizes the texture effect to the calculated lattice parameter. Thus, peak shifts towards lower and higher 2θ angles during boost and diffusion steps of the process are directly related to the change of the lattice parameter due to the presence of carbon as an interstitial element.

The carbon content dissolved in austenite can be calculated by using its' relation with the lattice parameter of austenite due to the occupation of octahedral sites of the austenitic lattice by carbon atoms. For this, Onink's model developed by using neutron diffraction experiments was used [11]. The model takes into account the thermal effect and gives the austenite lattice parameter as;

$$a_\gamma = (0.363067 + 0.000783x_C^r) \cdot [1 + (24.92 - 0.51x_C^r) \cdot 10^{-6} \cdot (T - 1000)] \qquad (1)$$

Where x_C^r is at. % carbon and T is the temperature in K. Using this approach the carbon content was calculated for the boost and diffusion steps. **Figure 3** shows the change of average carbon content dissolved in austenite during the boost and the diffusion steps for standard example. During the boost steps, the beam position was kept constant at the surface, i.e. the sample was stationary, while during the diffusion step the sample was scanned over 500 µm depth.

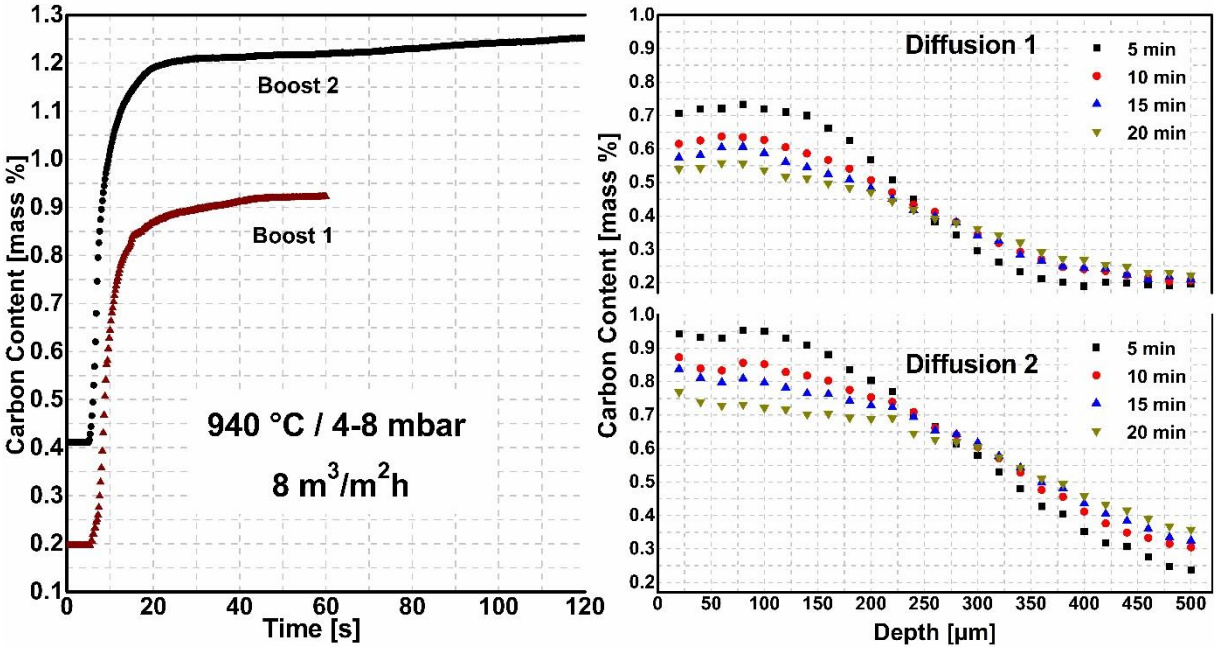

Figure 3: Evolution of carbon content dissolved in austenite during boost and diffusion steps. The measured region is averaging the beam area (20 x 1000 µm). Process temperature, pressure and acetylene flow rate are given in the figure respectively. All diffusion steps last 20 minutes at 0.1 mbar pressure under vacuum. Error bars are shorter than the symbol sizes.

According to **Figure 3**, during the boost steps, a high increase rate of carbon content at the first seconds and subsequent reduction in increase rate can be observed. The average carbon content increases from the nominal carbon content of about 0.2 ma. % up to about 0.87 ma. % for boost 1 and from 0.41 ma. % to 1.19 ma. % for boost 2 in the first 20 seconds. After that, the carbon content continues to increase very slowly until the end of each step to approx. 0.93 ma. % for boost 1 and 1.25 ma. % for boost 2. The determined

carbon content for the first boost steps is lower than the second and the third. This is because the measurements were made from the very surface to a depth of 20 µm (beam height); thus, the carbon content is the average value from the probed area, where saturation is not reached everywhere, even though the surface is saturated. This is more obvious for the first boost steps since there is no carbon gradient before.

Despite continuous acetylene supply into the furnace with the same rate during the entire boost step, carbon content reaches more or less a steady state concentration in the measured volume for both boost steps after 20 seconds. The reason for this is that acetylene decomposes to atomic carbon and gaseous hydrogen immediately when it comes in contact with the thermally activated metal surface under low pressure [12]. The limit for carbon transfer is the acetylene adsorption rate at the surface (free reaction sites for adsorption) and the diffusion rate of carbon from the surface into the bulk in austenite [13]. Free carbon diffuses therefore directly into the sample at a very high mass transfer rate in the early seconds of the boost step and accumulates in the austenite grains at the surface. When the maximum solubility is reached, a very fine cementite (Fe_3C) layer is formed in the first few microns of the surface. This could be demonstrated by these measurements [8].

Autocatalytic acetylene decomposition requires a hot metal surface, unlike propane which is a thermally decomposable gas and breaks down to its' constituents immediately after it enters the hot furnace. Therefore, the carbide layer formed at the surface of the sample might influence the acetylene decay negatively by blocking the reaction sides [14–16]. It is expected that carbon accumulation at the surface and carbide layer formation decelerate the carbon transfer from the atmosphere to the material. Diffusion in the material continues through the sample; however, in the present case, the probed region is from the surface to a maximum of 20 µm (beam height) which is highly affected by this accumulation and carbide formation. Therefore, a decrease of carbon content is not possible to observe. After 20 seconds, carbon content increase is only possible either via the dissolution of cementite or the limited amount of carbon diffusion through the cementite; on the other hand, a carbon decreasing effect is the diffusion of carbon through the core. Since the probed area is highly dominated by carbon accumulation and cementite formation, a decrease of carbon content due to diffusion is suppressed.

During both diffusion steps, the carbon content at the surface decreases faster at the beginning of the diffusion step and then the carbon diffusion in the depth slows down. This is due to the changing driving force provoked by the carbon concentration gradient which is the highest immediately after the boost step and continuously decreases.

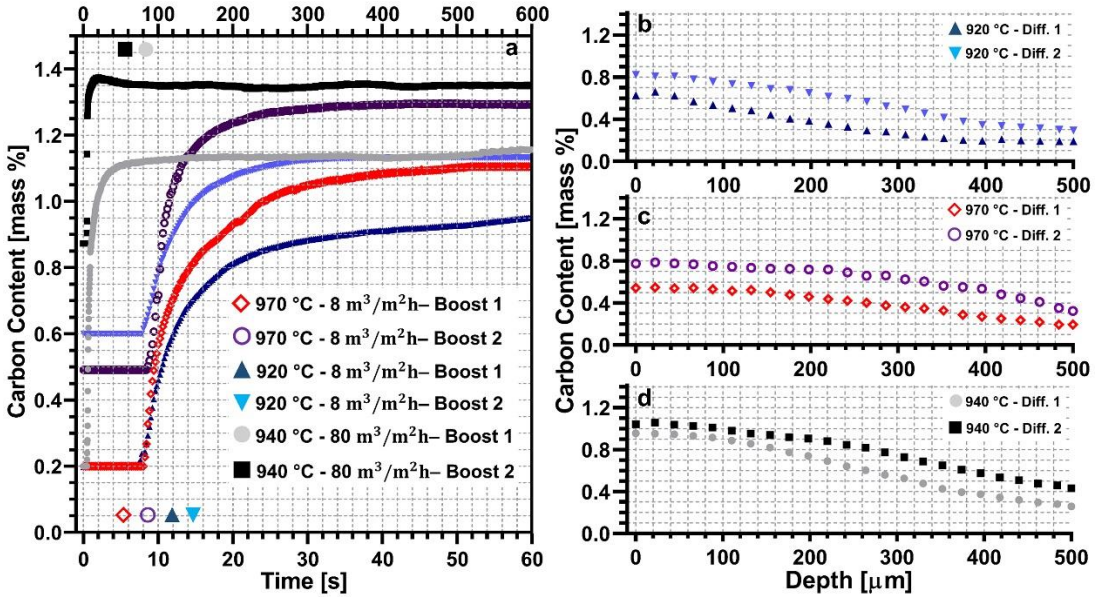

Figure 4: Evolution of the carbon content dissolved in austenite during the boost steps (a) and at the end of the diffusion steps (b, c, d) of the sample carburized with different process parameters. Symbols near each x-axis of the graph represent the lines belonging to that axis, which means the sample carburized at 940 °C has 600 sec of boost steps which is shown in the top x-axis. Process parameters are given on the graph. All diffusion steps last 20 minutes at 0.1 mbar pressure under vacuum.

Figure 4 show the change of carbon dissolved in austenite during boost and diffusion steps for samples carburized under different process conditions. As can be seen, during boost step (**Figure 4a**), regardless of process temperature, acetylene flow rate or boost step duration, the increase rate of the carbon content is higher in the early stage and then decreases during boost steps, and finally steady-state position is reached due to saturation of austenite. Although, increasing the temperature, retards this saturation, it is still reached the latest about 30 seconds for second boost steps. Moreover, increasing the temperature and acetylene flow rate has a positive effect on carbon dissolution in austenite during the boost step. In the diffusion step, similar to the boost step, the sample with a higher acetylene flow rate has a higher final carbon content in the depth of the sample. If the effect of temperature is compared (**Figure 4(b)** and **(c)**), increasing the temperature does not affect the near surface carbon content since the higher carbon absorption due to the higher temperature is compensated by higher diffusion speed caused by high temperature. Therefore, the carbon content through the depths is increased while the near surface carbon content is not affected by temperature.

It can also be noticed in **Figure 4(d)** that the near surface carbon content after the second boost step is very close to that after the first boost step which means the effect of the second boost step is quite low. This is attributed to the very fast carbide formation which retards the carbon diffusion from the atmosphere to the sample. These carbides could not dissolve completely during the following diffusion step. Therefore, further introducing acetylene in the

furnace in consecutive boost steps would only increase the amount of cementite formed at the surface, which also contributes to the overall carbon profile by dissolution. However, the effect of the contribution of cementite dissolution is very slow compared to direct contribution.

In order to confirm the carbide formation during the boost step, cementite diffraction peaks were observed. **Figure 5** shows some examples of X-ray patterns of γ {111} austenite peak and small cementite peaks for samples with different surface carbon content. Broader peaks are mainly due to carbon gradient in the measured area which causes a different magnitude of expansion in austenite lattice.

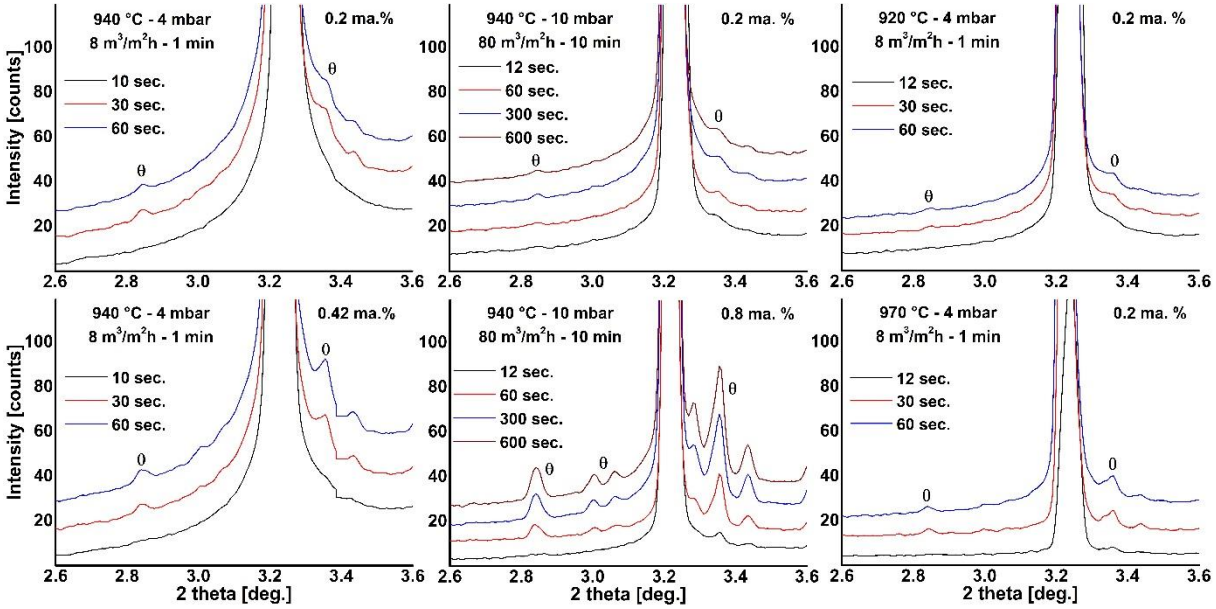

Figure 5: Diffractograms showing growth of small cementite (Fe3C / θ) peaks near the main γ {111} austenite peak during different stages of boost steps of samples carburized with different process parameters. Each process parameter is shown in the top left corner and initial surface carbon content are shown in the top right corner. Time at the left side shows duration from the beginning of the boost step. Lower peaks were taken as a reference. Each peak after these was offset +5 cts from the previous one to distinguish easily.

As it can be seen from the figure, carbides are formed during the boost step after austenite saturation for all samples carburized with different process parameters. Small carbide peaks are visible already after 12 seconds for the samples with higher acetylene flow rates while samples with lower flow rates show peaks around 30 seconds. Saturation of the austenite at the surface is assumedly only 2-3 µm from the top since the average carbon content at the probed beam area is lower than the maximum solubility limit of austenite (approx. 1.30 ma. % for 940 °C) especially for the first boost steps which is an indication of a significant carbon gradient. Additionally, compared to main γ {111} austenite peaks heights, cementite peaks are very small. Since measurements were made from surface to approximately 20 µm depth, only the first microns of this probed area should be saturated and formed cementite.

3.2. Quenching step

After the desired number of boost diffusion cycle was reached, the temperature was lowered to the hardening temperature (about 840°C) for all samples to reduce the distortion due to quenching. After the sample was kept for several minutes at hardening temperature for temperature homogenization, it was quenched with 5 bar Helium gas until 80 °C reached. Below 80 °C, the helium quench gas was stopped and the samples cooled down slowly to room temperature

Figure 6 shows the change of integrated diffraction frame of the γ {111} austenite peak during quenching and the formation of martensite by the appearance of the α' {110}\{101} martensite peak for the standard experiment as an example (see **Table 1**). During quenching, γ {111} austenite peak shifts to higher angles very sharply due to lattice shrinkage caused by the strong temperature decrease and α' {110}\{101} martensite peaks start to appear at about 205 °C.

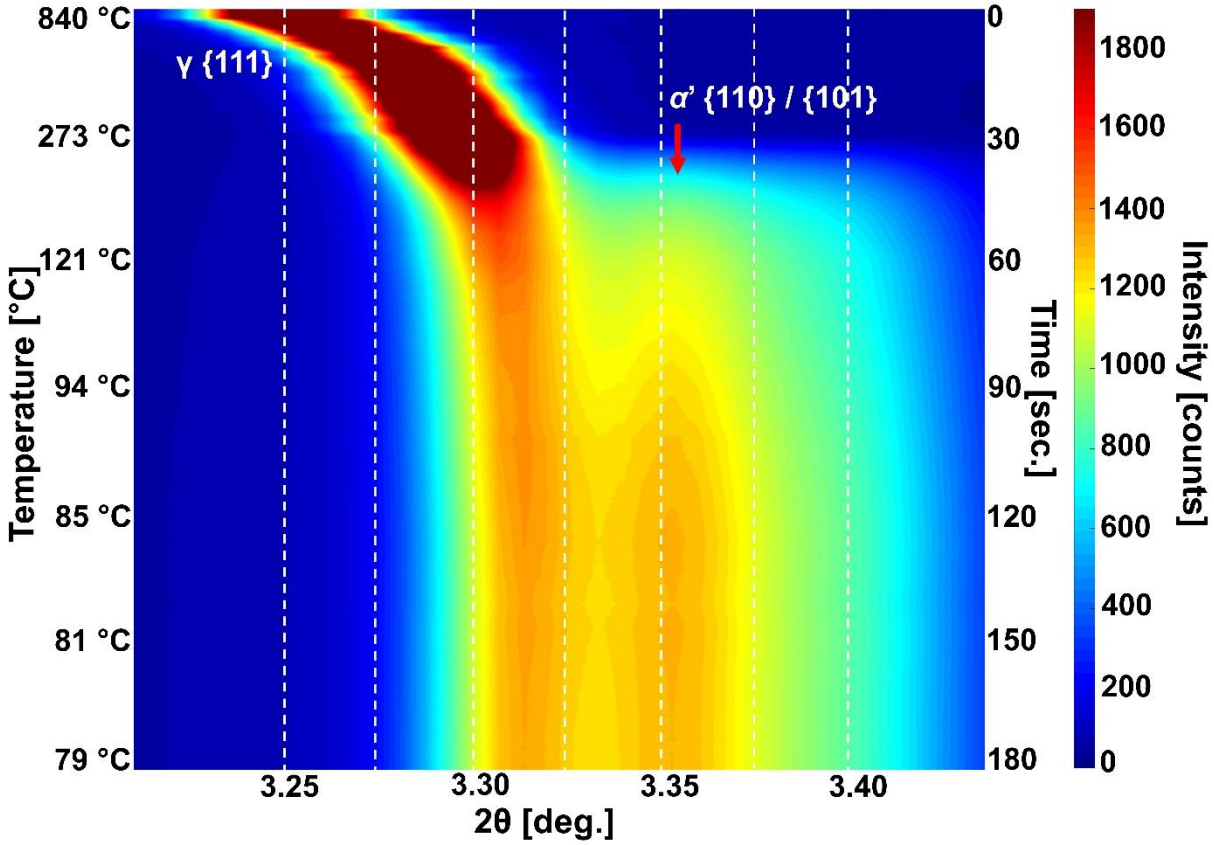

Figure 6: Temporal evolution of diffraction patterns to illustrate the shifting of the γ {111} austenite peak to higher angles and the formation of the α´ {110}/{101} double martensite peak during quenching. Process temperature was 940 °C. Duration of boost-diff. cycles before quenching were 1-20 min, 2-20 min and 1-25 min, respectively.

Precise phase fractions in the near-surface region during quenching was obtained by using Rietveld analysis of the diffraction patterns. **Figure 7** shows the evolution of austenite and martensite as a function of temperature. As can be seen, after the first 10 seconds, the measured temperature is 470 °C which gives a quenching rate of about 30 °C/s. This rate

reduces exponentially until 80 °C was reached. This sample was carburized at 940 °C with 3 consecutive boost steps having 1 min, 2 min. and 1 min. duration. Diffusion steps between the boost steps were 20 min., 20 min. and 25 min. respectively (see **Table 1**).

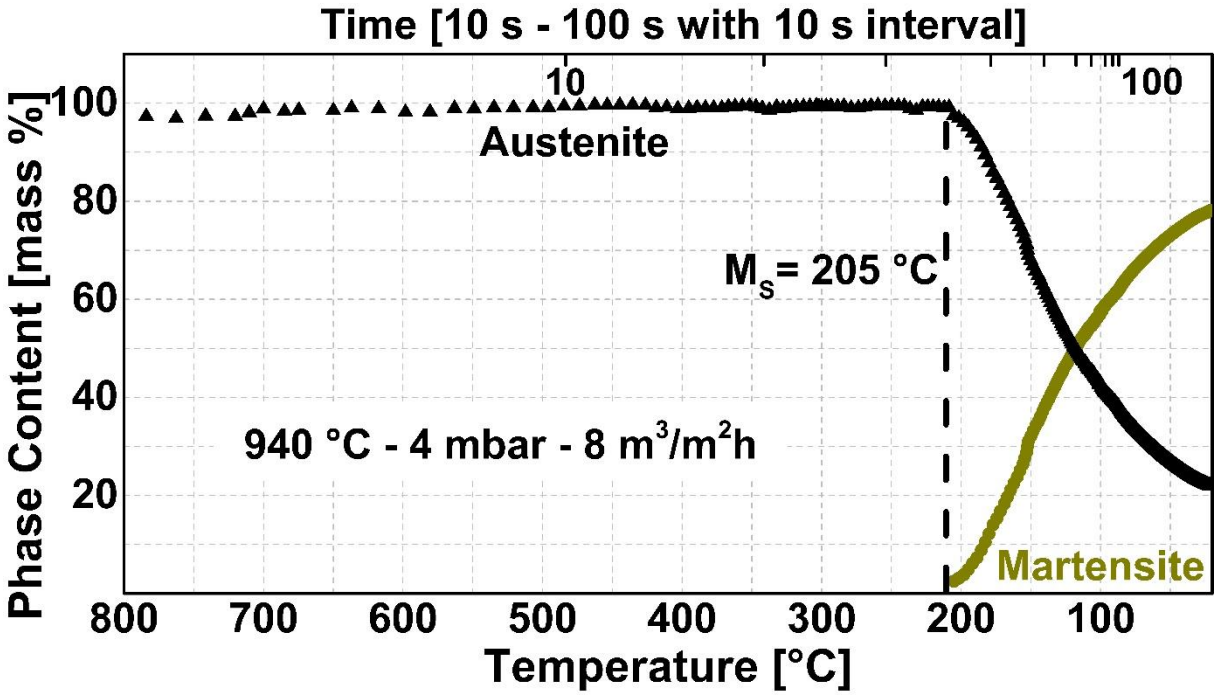

Figure 7: Evolution of the phase content during quenching over temperature and time. Process parameters are given in the figure. The top x-axis represents each 10 seconds interval until 80 °C to show an exponential change of the cooling rate.

It can be seen from in-situ data that the first martensite phase appears at 205 °C (Ms temperature) which is an indication of a high carbon content dissolved in austenite. This high carbon content retarded the bainite transformation; therefore, no transformation can be observed until the Ms reached despite the moderate cooling rate.

The linear relationship between the tetragonality and the carbon content in martensite given in **Equation 2** was used to determine the carbon dissolved in martensite [17].

$$c/a = 1 + 0.045x_C \qquad (2)$$

Other alloying elements such as chromium and manganese substitute iron so they only have a minor effect on the c/a ratio of martensite. Since the ratio of both lattice parameters is considered, the effect of temperature is mostly self-compensating [18].

Figure 8 shows the evolution of the determined carbon content as well as the lattice parameter of martensite calculated using **Equation 2** over the temperature for the same standard sample as an example.

In the first 3 seconds, until 185 °C, the lattice parameter “c” increases steeply and then increase rate reduces, while the lattice parameter “a” decreases with also high rate and then continues to decrease with a very low rate. After 60 seconds, both values stay constant until the end of the step.

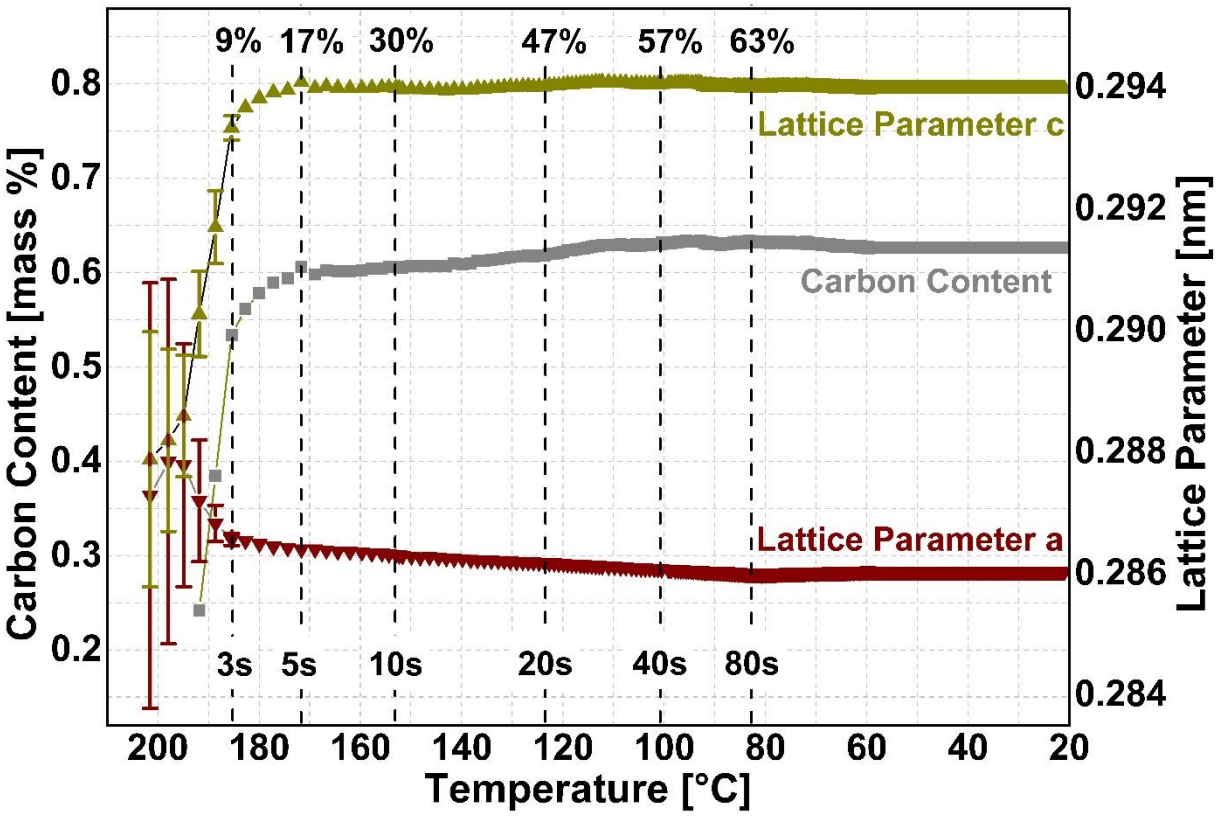

Figure 8: Evolution of lattice parameters of martensite and the carbon content in solution for martensite as a function of temperature. The dotted vertical lines show the amount of martensite in mass % at the top and the time from the beginning of quenching in seconds at the bottom.

The c/a-ratio, i.e. the tetragonality of the martensite, increases during the transformation. In the first 3 seconds, error margins are wide due to the low amount of martensite; however, between the 3rd and the 5th seconds, measurements and fits are more precise due to the higher amount. One possible reason of lower tetragonality in early stages might be the preferential transformation of regions with lower carbon content, for example near precipitates or near grain boundaries. Moreover, this behaviour might also be attributed to a phenomenon of the direct ordering of carbon atoms within the lattice at high temperature (Zener ordering), as well as an instantaneous self-tempering effect of martensite, which is more pronounced in the first stage of the transformation due to the higher temperature [19].

Martensitic transformation possesses both chemistry and internal stress changes. Thus, estimation of the carbon content solely with an XRD study is generally limited to semi-quantitative conclusions based on assumptions that make certain judgements about the carbon partitioning kinetics difficult. Nonetheless, if the XRD results are combined with

literature studies that are based on complementary characterization techniques, reliable statements might be deduced.

Transformation of martensite is generally considered as diffusionless transformation, i.e. carbon partitioning is usually neglected because of very low temperatures and rapid transformation. However, previous studies show evidence contrary to this idea. For example, carbon partitioning from martensite to retained austenite during quenching [19–24]; especially for cooling rates below 25 K/s [23] is highly reported in the literature. In the present in-situ study, the average cooling rate until Ms temperature during quenching was about 17 K/s (see **Figure 7**), and further reduced to lower values below Ms, which correlates with literature. Even for very low Ms, like in the present study, the minor effect of carbon partitioning from martensite to retained austenite could be observed [19]. Additionally, segregation of carbon to the microstructural features like dislocations or martensite lath boundaries is also highly stated in various studies, especially for the cases that lower Ms restricts the mobility of carbon [25–27]. Therefore, based on the combination of the present results and results from the literature, carbon partitioning from supersaturated martensite to microstructural features during martensitic transformation is the most convincing among others. However, it should be kept in mind that carbon partitioning from martensite to retained austenite is also possible to a small extend.

4. Conclusion

Synchrotron X-ray diffraction experiments were performed on beamline P07-EH3 of Petra III at DESY/Hamburg during the whole low pressure carburizing process and final quenching with the newly developed process chamber. A series of experiments were conducted, while process parameters such as the temperature, the duration of the process steps and the amount of acetylene flow were systematically varied. Collected data were analysed by using the convolution-based Rietveld refinement and experimental based mathematical calculations to obtain information about the microstructural evolution.

Carbon saturation in austenite was reached in the early stages of the boost step for all processes due to the very fast carbon uptake rate from the atmosphere into the sample. After that, the accumulation of carbon atoms at the surface caused immediate carbide precipitation confirmed by cementite peaks that appeared near the main γ {111} austenite peak. Therefore, the direct contribution of carbon donor gas to the carbon profile was reduced to very low levels. After that point, further supply of carbon donor gas increased the amount of carbides formed at the surface which will contribute to the carbon profile indirectly by dissolution in the following diffusion steps. Moreover, increasing the process temperature and acetylene flow rate increased the carbon dissolved in austenite during the boost step. For the case of carbide formation, increasing the acetylene flow rate clearly increased the

content of carbides formed at the surface; however, the effect of temperature on carbide formation was not as distinct and as flow rate.

Additionally, during quenching, early formed martensite, especially martensite that was formed in the first 5 seconds, had a lower c/a ratio than later formed ones. The main reason of this was not determined. However, this difference was attributed to the early phase transformation of austenite grains having lower carbon content. On the other hand, it is also possible that instantaneous self-tempering and carbon redistribution/ordering leading to lower tetragonality might take place.

Acknowledgement

The authors gratefully acknowledge the support from the Deutsche Forschungsgemeinschaft (DFG) for funding this research under the collaborative project EP-128/2-1- | GI-376/15-1 (DFG project no. 399551201), Deutsches Elektronen-Synchrotron (DESY) for granting beam time. Furthermore, the authors would like to thank Alexander Kohl and Sebastian Ohneseit for their participation in the measuring campaign at DESY and in particular Alexander Kohl for his engagement in the planning and realization of the process chamber.

References

1. Clausen, B.; Hoffmann, E.; Zoch, H.W.: Beeinflussung der Randschicht Durch die Einsatzhärtung. HTM - J. Heat Treat. Mater. 63 (2008) 6, pp. 326–336, DOI:10.3139/105.100473
2. Starck, A. von; Mühlbauer, A.; Kramer, C.: Handbook of Thermoprocessing Technologies: Fundamentals, Processes, Components, Safety. Vulkan-Verlag GmbH, Essen (2005) pp. 509
3. Altena, H.; Schrank, F.: Low Pressure Carburizing with High Pressure Gas Quenching. In: Gear Technology. Heat Treating (March/April 2004)
4. Edenhofer, B.: An overview of advances in atmosphere and vacuum heat treatment. Heat Treat. Met. 26 (1999) 1, pp. 1–5,
5. Gräfen, W.; Edenhofer, B.: New developments in thermo-chemical diffusion processes. Surf. Coatings Technol. 200 (2005) 5–6, pp. 1830–1836, DOI:10.1016/j.surfcoat.2005.08.107
6. Kula, P.; Pietrasik, R.; Dybowski, K.: Vacuum carburizing - Process optimization. J. Mater. Process. Technol. 164–165 (2005) 2, pp. 876–881, DOI:10.1016/j.jmatprotec.2005.02.145
7. Prunel, G.; Stauder, B.: Advantages of low pressure carburizing in the heat treatment. Cailiao Rechuli Xuebao/Transactions Mater. Heat Treat. 25 (2004) 5, pp. 364–369,
8. Tapar, O.B.; Epp, J.; Steinbacher, M.; Gibmeier, J.: In-situ synchrotron X-ray diffraction investigation of microstructural evolutions during low pressure carburizing. Metall. Mater. Trans. A Phys. Metall. Mater. Sci. 52 (2021) 4, pp. 1–16, DOI:10.1007/s11661-021-06171-2
9. Ashiotis, G.; Deschildre, A.; Nawaz, Z.; Wright, J.P.; Karkoulis, D.; Picca, F.E.; Kieffer, J.: The fast azimuthal integration Python library: PyFAI. J. Appl. Crystallogr. 48 (2015)

2, pp. 510–519, DOI:10.1107/S1600576715004306

10. Coelho, A.A.: TOPAS and TOPAS-Academic: An optimization program integrating computer algebra and crystallographic objects written in C++: An. J. Appl. Crystallogr. 51 (2018) 1, pp. 210–218, DOI:10.1107/S1600576718000183

11. Onink, M.; Brakman, C.M.; Tichelaar, F.D.; Mittemeijer, E.J.; van der Zwaag, S.; Root, J.H.; Konyer, N.B.: The lattice parameters of austenite and ferrite in FeC alloys as functions of carbon concentration and temperature. Scr. Metall. Mater. 29 (1993) 8, pp. 1011–1016, DOI:10.1016/0956-716X(93)90169-S

12. Esper, B.: Acetylene: The Right Carbon Source For Low-Pressure Carburizing. Ind. Heat. November (2009)

13. Steinbacher, M.: Thermogravimetrische Messungen beim Niederdruckaufkohlen als Grundlage für Simulationen. Universität Bremen. PhD Thesis (2012)

14. Daniel H. Herring; Robert V. Peters Jr.: New-Formula Acetylene Cool for Heat Treatment. Gear Technol. (September 2013)

15. Madix, R.J.: Reaction Kinetics and Mechanism on Metal Single Crystal Surfaces. Adv. Catal. 29 (1980) pp. 1–53, DOI:10.1016/S0360-0564(08)60119-4

16. Neubauer, R.; Whelan, C.M.; Denecke, R.; Steinrück, H.P.: The thermal chemistry of saturated layers of acetylene and ethylene on Ni(100) studied by in situ synchrotron x-ray photoelectron spectroscopy. J. Chem. Phys. 119 (2003) 3, pp. 1710–1718, DOI:10.1063/1.1582432

17. Bhadeshia, H.K.D.H.; Honeycombe, R.W.K.: Steels: Microstructure and Properties: Fourth Edition. Elsevier Inc, Amsterdam (2017), pp. 142

18. Lu, Y.; Yu, H.; Sisson, R.D.: The effect of carbon content on the c/a ratio of as-quenched martensite in Fe-C alloys. Mater. Sci. Eng. A. 700 (2017) pp. 592–597, DOI:10.1016/j.msea.2017.05.094

19. Epp, J.: Time Resolved Investigations Of Phase Transformations and Stress During Heat Treatments of Steel Samples by Meams of Diffraction Experiments. Ph.D. Thesis, Bremen (2016) DOI:10.2370/9783844045475

20. Bhadeshia, H.K.D.H.: Carbon content of retained austenite in quenched steels. Met. Sci. 17 (1983) 3, pp. 1–2, DOI:10.1179/030634583790421087

21. Lerchbacher, C.; Zinner, S.; Leitner, H.: Atom probe study of the carbon distribution in a hardened martensitic hot-work tool steel X38CrMoV5-1. Micron. 43 (2012) 7, pp. 818–826, DOI:10.1016/j.micron.2012.02.005

22. Sarikaya, M.; Thomas, G.; Steeds, J.W.; Barnard, S.J.; Smith, G.D.W.: Solute Element Partitioning and Austenite Stabilization in Steels. (1982) DOI:10.2172/7031961

23. Sherman, D.H.; Cross, S.M.; Kim, S.; Grandjean, F.; Long, G.J.; Miller, M.K.: Characterization of the carbon and retained austenite distributions in martensitic medium carbon, high silicon steel. Metall. Mater. Trans. A Phys. Metall. Mater. Sci. 38 (2007) 8, pp. 1698–1711, DOI:10.1007/s11661-007-9160-3

24. Thomson, R.C.; Miller, M.K.: An atom probe study of carbon distribution in martensite in 2 1/4 Cr1Mo steel. Scr. Metall. Mater. 32 (1995) 2, pp. 149–154, DOI:10.1016/S0956-716X(99)80028-4

25. Morsdorf, L.; Tasan, C.C.; Ponge, D.; Raabe, D.: 3D structural and atomic-scale analysis of lath martensite: Effect of the transformation sequence. Acta Mater. 95 (2015) pp. 366–377, DOI:10.1016/j.actamat.2015.05.023

26. Wilde, J.; Cerezo, A.; Smith, G.D.W.: Three-dimensional atomic-scale mapping of a Cottrell atmosphere around a dislocation in iron. Scr. Mater. 43 (2000) 1, pp. 39–48, DOI:10.1016/S1359-6462(00)00361-4

27. Zhu, C.; Cerezo, A.; Smith, G.D.W.: Carbide characterization in low-temperature tempered steels. Ultramicroscopy. 109 (2009) 5, pp. 545–552, DOI:10.1016/j.ultramic.2008.12.007